

Dynamics of Chromosome Compaction during Mitosis

Abhijit Sarkar,^{*1} Sertac Eroglu,[†] Michael G. Poirier,^{*} Prateek Gupta,[†] Ajay Nemani,^{*} and John F. Marko^{*†}

^{*}Department of Physics, 845 W. Taylor Street, and [†]Department of Bioengineering, 851 S. Morgan Street, University of Illinois at Chicago, Chicago, Illinois 60607-7059

We have quantitatively studied the space-time dynamics of mitotic chromosome compaction in cultured amphibian cells. After collecting digital phase-contrast images we have done digital image analysis to study spatial correlations in density. We find a characteristic distance at which the strongest correlations occur, which provides a quantitative measure of the size of patches of dense chromatin during interphase and early prophase. Later in mitosis, this length corresponds to the thickness of prophase and metaphase chromosomes. We find that during interphase strong correlations exist at a few-micrometer length; during prophase this correlation length progressively drops as the chromosomes are compacted. Our data are explained by a model based on assembly of chromatin loops onto already fiberlike interphase chromosomes. To test this model we have microinjected cobalt hexamine trichloride into interphase nuclei and have observed the rapid condensation of the interphase chromatin into thick fibers with a spacing similar to the native-state interphase correlation length determined from our image analysis. © 2002 Elsevier Science (USA)

Key Words: chromosome structure; chromosome condensation; mitosis.

INTRODUCTION

The spatial organization of chromosomes and how chromosome organization changes during the cell cycle are incompletely understood. It has been shown that during interphase different chromosomes are confined in different nuclear “territories” [1], that individual chromosomes show random-walk correlations along their length [2], and that some chromosome loci are anchored to or near the nuclear envelope [3] and perhaps to nuclear structures such as the “nuclear matrix” [4]. However, the questions of how chromosome structure is reorganized during mitosis and how large-scale chromosome structure during interphase and mitosis

are related remain unanswered. Even the large-scale structure of mitotic chromatids remains controversial [5–7], with some groups favoring folding of chromatin loops onto a central protein axis [8], while others suggest successive levels of helical folding [9].

Here we focus on quantification of the evolution of chromosome structure from dispersed chromatin during interphase into the condensed, micrometer-thick chromatids of mitosis. Before mitosis, the chromosomes replicate inside the nucleus (in the cells of this study, an ellipsoidal cell organelle with a diameter of $\approx 40 \mu\text{m}$ and a thickness of $\approx 16 \mu\text{m}$); during this process the nucleus volume increases to accommodate the doubling in chromosome mass. During all of interphase, including during DNA replication, the chromosomes are too thin to be visible as separate fibers using light microscopy.

During prophase, the first stage of mitosis, there is no significant change in the overall shape and size of the nucleus. However, inside the nucleus, the compacting chromosomes gradually become thick enough to be visible in the light microscope (for the cells of this study up to $\approx 2 \mu\text{m}$ thick). The chromosomes first appear as a striped pattern in the nucleus, suggesting a two-dimensional organization (see below). We present a quantitative analysis of this chromosome reorganization, from the beginning of prophase (Fig. 1a) to the dissolution of the nuclear envelope and the beginning of pro-metaphase (Fig. 1e).

We use Fourier analysis, which breaks the complicated images of the nucleus up into simple periodic (light–dark) components. Each Fourier component is a spatial wave and is characterized by a wavelength and an amplitude. By computing the power spectrum of the Fourier components (the square of the amplitude, averaged over wave direction) as a function of wavelength, we can measure the length scale at which correlations are most strong. This technique is widely used for analysis of dynamics of phase transitions [10].

We have found that at all stages of chromosome compaction, including during interphase, the spatial power spectrum has a pronounced peak for components with a wavelength of a few micrometers. The amplitude of the power spectrum at its peak is almost as

¹ To whom reprint requests should be addressed at Department of Physics, University of Illinois at Chicago, 845 W. Taylor Street, Chicago, IL 60607-7059. Fax: (312) 996-9016. E-mail: asarkar@callan.phy.uic.edu.

large during interphase as that during later stages. Thus, chromatin density is strongly correlated over a distance of a few micrometers at all stages of the cell cycle. During interphase and early prophase, this correlation is due to “patches” of chromatin density.

Later in prophase and into metaphase, the correlation distance measures the spacing of the chromosomes themselves. We find that the correlation length progressively decreases from its interphase value as chromosome compaction occurs during prophase. This is distinct from usual “condensation” processes (e.g., phase separation of two immiscible liquids [10] which show a gradual *increase* in correlation length corresponding to gradual growth of “bubbles” of the separating phases). Instead, the presence of strong chromatin density correlations in interphase and the decrease in correlation length during prophase suggest that chromatin is compacted onto an already fiberlike interphase chromosome.

The result that there are similar correlation lengths for chromatin density inhomogeneities during interphase and prophase suggested that it might be possible to effect artificial chromosome compaction by the use of trivalent cations (cobalt hexamine trichloride) which are known to cause DNA and chromatin aggregation at relatively low concentration [11]. We thus microinjected live interphase nuclei with this cation and observed the kinetics of the response of the chromatin density. We found that the chromatin reorganizes on the ≈ 1 -s time scale into filamentous bundles separated by apparent voids. The spacing of these bundles is roughly the same as that of the wavelength associated with the native interphase chromatin correlation length.

These experimental results suggest that during prophase, chromatin domains unfolded during interphase are simply compacted onto a central chromosomal filament. This explains how similar results can be obtained by analysis of the orderly chromosome compaction during normal cell division and abrupt chemical condensation of chromatin by trivalent ions. To further support this idea we present a calculation of the density correlations predicted by a model where interphase chromosomes and metaphase chromosomes have a similar fiberlike structure, differing only in the degree of compaction of chromatin domains; we show that such a model can reproduce our experimental results.

MATERIALS AND METHODS

Cell culture. We studied two types of newt (*Notophthalmus viridescens*) cells: (a) lung epithelial cells explanted from animals [12] and (b) cultured TVI epithelial cells [13]. The morphology of the two cell types does not differ significantly. We use this species because of its large chromosome size, which greatly aids in visualization of chromosome compaction. Standard amphibian cell culture tech-

niques were used [13] to grow the cells in a monolayer on the bottom of culture dishes. The dishes (Falcon) were prepared by having their bottoms cut out and replaced with circular No. 1 cover glasses (Fisher). The glass bottoms were glued on using molten wax.

Video microscopy. An inverted microscope (Olympus IX-70) with a 60X 1.25 N.A. objective (Olympus UPHFL-60) and a video camera (Panasonic WV-BP 310) were used to image the cells. Acquisition of digital images was done with a frame grabber (National Instruments IMAQ-4.1) directly to hard disk on a PC. The PC also controls in-plane (x - y) and focus plane (z) positions using an x - y - z positioning system (H128 Series Motor Controller from Prior Scientific Instruments Ltd.). Phase-contrast imaging was used throughout this study, in which darker regions are those with a higher net density of protein and nucleic acid. Analogous results were obtained using DIC imaging.

Chromosome compaction image acquisition experiments. To collect data on native chromosome compaction, we selected a cell which appeared to be in the earliest stages of cell division, i.e., a cell with a large, rounded nucleus. Often such cells do not divide, but after ≈ 10 trials, we obtained data starting from a point preceding the onset of visible chromosome compaction. Every 5 min, a Labview control program on the PC focused the microscope through $20 \mu\text{m}$, in steps of $0.2 \mu\text{m}$, to produce a 3D image “stack,” with a total stack acquisition time of 20 s. Over the few-hour duration of a typical experiment, we thus collected roughly 50 image stacks. Following the experiment, the image stacks were cropped to include only the nucleus for further analysis. In addition to this 3D + time data we acquired a variety of (2D) images of nuclei and cytoplasm, mainly for use as control data (see below).

Image analysis. To understand the gross spatial organization of compacting chromosomes we reconstructed them by volume rendering of cropped 3D data using the software package VOLPACK (see <http://graphics.stanford.edu/software/volpack> for software) (Fig. 1g). Quantitative study of the correlations in images was done using Fourier analysis of the images. This amounts to decomposition of the complicated images into a sum of periodic density waves, each of which is described by a wavelength, a direction, and an amplitude. From the amplitudes, we computed a power spectrum as a function of wavelength, which indicates the relative weight of the various wavelength fluctuations in the original image. To simplify the power spectra we averaged over the direction of the density modulation, resulting in a power spectrum which depends on wave number k (inverse wavelength) alone.

From image data $\rho(\mathbf{r})$, we compute the direction-averaged power spectrum

$$S(\mathbf{k}) = |\rho(\mathbf{k})|^2, \quad (1)$$

where

$$\rho(\mathbf{k}) = \int d\mathbf{r} \exp(-i\mathbf{k} \cdot \mathbf{r}) \rho(\mathbf{r}). \quad (1a)$$

Here k is the wave number, equal to $2\pi/l$, where l is the Fourier component wavelength. The power spectrum is averaged over all directions ϕ in the plane, to obtain a circularly averaged result:

$$S(k) = \frac{\int d\phi S(\mathbf{k})}{\int d\phi}, \quad (2)$$

where ϕ is the direction of k in the plane. We extract an estimate of the wavenumber k^* at the peak using

$$k^* = \frac{\int k S(k) dk}{\int S(k) dk}. \quad (3)$$

This calculation is an average of wavenumber, weighted by the power spectrum amplitude, and gives a k^* near the peak of the spectrum. From k^* the characteristic wavelength, or correlation length, follows as $l^* = 2\pi/k^*$. The wavelength l^* indicates the range of correlation of light and dark patches in the images. For the noodlelike chromosome patterns, this corresponds to the center-to-center distance between adjacent chromosomes, or roughly double the chromosome thickness.

Microinjection experiments. Chemicals were introduced into live cell nuclei using glass micropipettes fabricated with a $\approx 1\text{-}\mu\text{m}$ inside diameter. Pipettes were pulled from 1-mm OD, 0.75 mm ID glass capillaries (World Precision Instruments) using a commercial puller (Sutter Instruments). They were cut to have the desired diameter using a homemade forge consisting of a 100- μm -diameter platinum wire (Fisher) attached to an adjustable low-voltage power source, mounted to the stage of a microscope.

Cut pipettes were then mounted into a pipette holder (Narishige) prefilled with the solution to be injected, using suction. Once filled, they were mounted in a motorized micromanipulator (Sutter Instruments MP-285) mounted on the IX-70 microscope and attached to a microinjection pump (World Precision Instruments PV-83 Pneumatic Pico Pump). The pipette was then pushed through the membrane of a cell and brought to the edge of the nucleus. Injection was then done for 5 s using 100 Pa of pressure. Microinjection experiments were done with 5 mM cobalt hexamine trichloride (Fluka), in 60% PBS (BioWhittaker). Image data were taken by the PC at a rate of about two frames per second during microinjection.

RESULTS

Chromosomes are organized in a plane during mitotic compaction. Figures 1a–1f show a few images from the middle of image stacks at a few times during one cell division. In these images the chromosomes can be seen to organize from a patchy preprophase nucleus to prophase fibers and then into individual chromosomes. To understand the organization of the prophase chromosomes, image stacks were reconstructed into renderings of 3D objects using VOLPACK. The reconstructed chromosomes (Fig. 1g) have a quasi-2D organization like a layer of noodles confined to the central nuclear plane. This indicated to us that we should carry out 2D Fourier analysis on images cutting the central nuclear region of the cell. Additional analysis using 3D Fourier analysis produced similar results (not shown).

Chromatin power spectrum has a strong peak. In experiments where time series were taken through mitosis, we found strong correlations at all mitotic stages. Figure 2 shows $S(k)$ determined from central cell planes (similar to those shown in Figs. 1a–1f) in one of the experiments. The range of wave number shown is from 0 to 5 μm^{-1} , which corresponds to wavelengths larger than $2\pi/5 = 1.3 \mu\text{m}$. Thus, the range of wave numbers shown corresponds to wavelengths at which our microscope objective is able to resolve detail (objectives with N.A. > 1 are able to resolve details larger than 0.5 μm , roughly the wavelength of visible light).

A pronounced peak can be seen each prophase time step (90, 100, and 120 min, respectively) for $k \approx 1.5$

μm^{-1} . This corresponds to modulations in density with wavelength $\approx 2\pi/1.5 = 4 \mu\text{m}$. Comparison with the prophase images (Figs. 1c and 1d) shows that this wavelength corresponds to the spacing of adjacent prophase chromosomes.

During prophase there is a gradual shift in the peak position to larger wave number, indicating that the typical distance over which the chromatin density is correlated is going down as the chromosomes are being compacted. The amplitude of $S(k)$ also gradually increases during prophase, indicating an overall increase in contrast between sparse and dense regions of chromatin as chromosome compaction occurs.

Figure 2 also shows $S(k)$ during interphase (20 min). A strong peak is found at $k \approx 1 \mu\text{m}^{-1}$, indicating strong correlations in density over $\approx 6 \mu\text{m}$. This corresponds to the size of “clumps” or “patches” of chromatin in interphase nuclei (Fig. 1a) and led us to compare with results from other randomly selected interphase cells (see below).

Finally, $S(k)$ during metaphase (Fig. 2, 135 min) shows a large peak near $k \approx 1 \mu\text{m}^{-1}$. This corresponds to the $\approx 5\text{-}\mu\text{m}$ spacing between adjacent chromosomes (Fig. 1f). The high contrast between the metaphase chromosomes as a whole and the surrounding cell gives rise to the large amplitude at the smallest wave number.

Time evolution of peak position of $S(k)$. From Fig. 2 it can be seen that the peak position of $S(k)$ shifts toward larger wave number k during prophase, as the chromosomes are compacted (Fig. 2). To make this more definite we computed the power spectrum-weighted wave number (k^*) and from this computed the characteristic wavelength $l^* = 2\pi/(k^*)$. This wavelength l^* is shown in the Fig. 2 inset as a function of time, for data from three separate experiments. The time scales have been shifted so that the breakdown of the nuclear envelope at the end of prophase occurs at 120 min for each case.

Until the end of interphase, the characteristic length l^* is essentially constant (Fig. 2, inset) and is nearly the same value in different cells. Then, in prophase, l^* gradually decreases as the chromosomes compact. Finally, when the nuclear envelope disappears at the beginning of metaphase, l^* rapidly increases. This is because the chromosomes move apart when the nucleus opens, increasing the typical distance between chromosomes which dominates the calculation of l^* .

Peak position of $S(k)$ is nearly constant during interphase. Figure 2 shows that during late interphase l^* is nearly constant and almost the same in different cells. Additional measurements on other interphase cells give a similar peaked $S(k)$ (Fig. 3, solid line), with values in the range $3.8 \pm 0.4 \mu\text{m}$. Thus, interphase

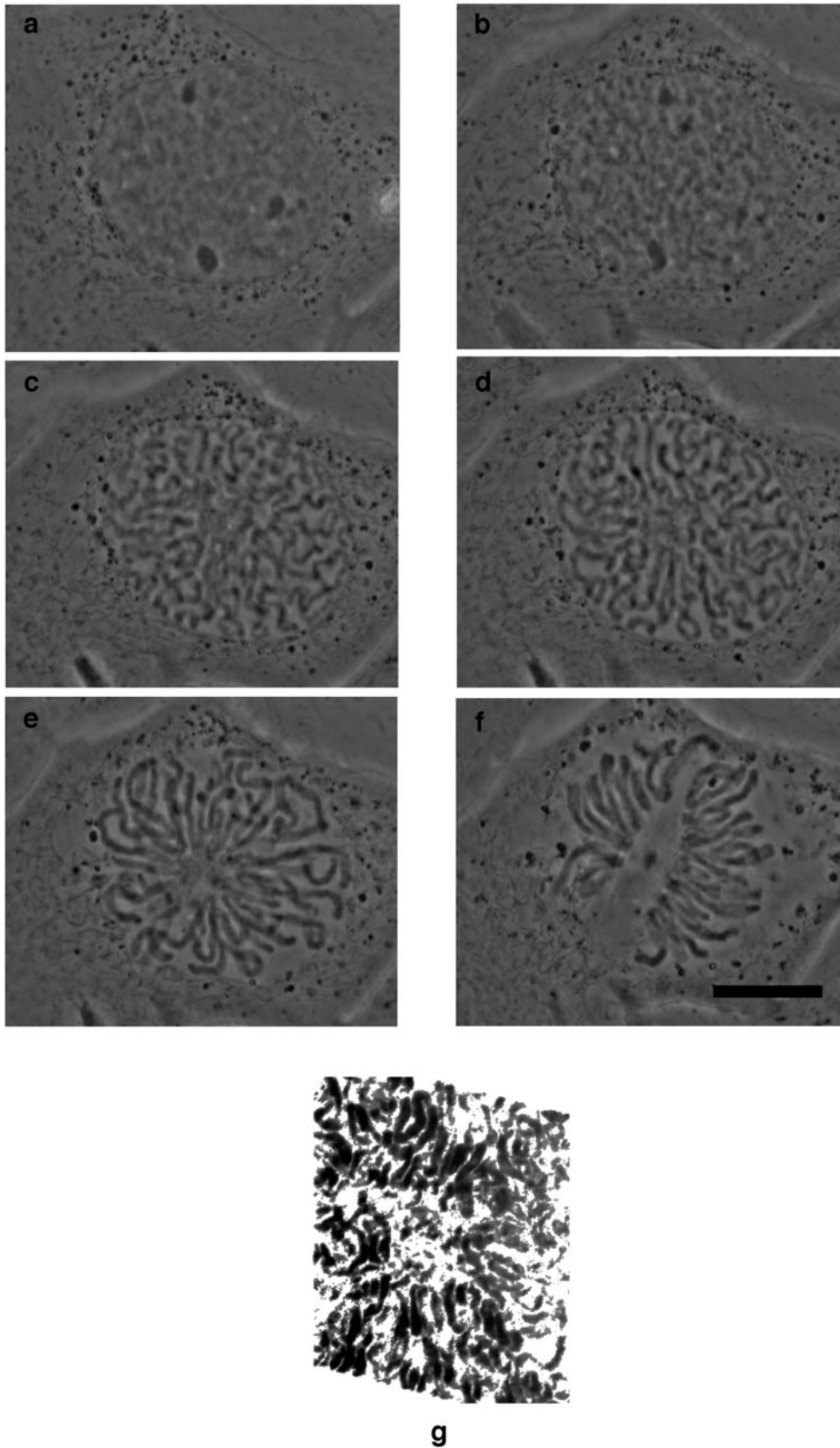


FIG. 1. Organization of chromosomes in mitosis. Computer-aided reconstruction of (prophase) chromosomes from phase-contrast sectioning microscopy data strongly suggests that the packing is two dimensional (g). The evolution of global multichromosome morphology during mitosis from "homogeneous" phase (a) to noodlelike phase (e, late prophase) and final separated and aligned pro-metaphase chromosomes (f) is shown. Bar is 20 μm .

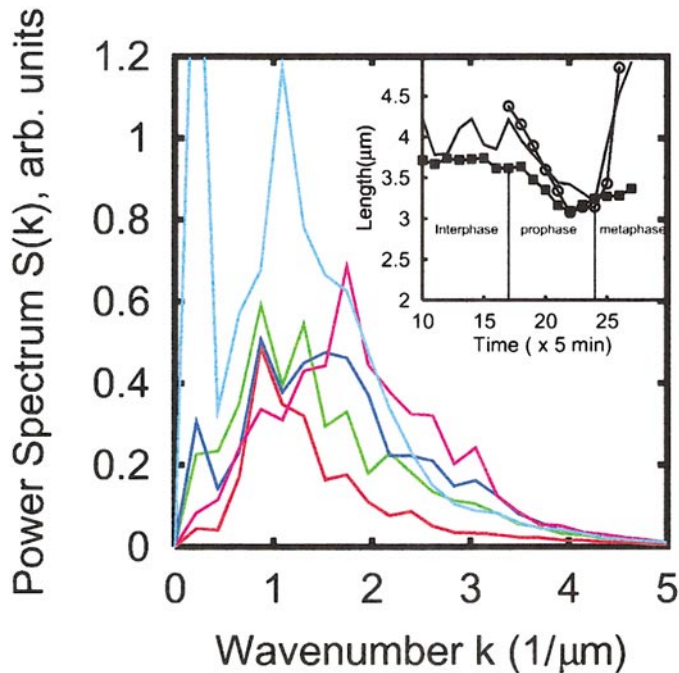


FIG. 2. Evolution of chromosome spatial correlations during the cell cycle. $S(k)$ for five time points (20, 90, 100, 120, and 135 min) of a nucleus beginning with mid-interphase (red) to just before onset of mitosis (green) to mid-prophase (purple) to just preceding the end of prophase (pink) and, finally, pro-metaphase/metaphase (blue). The rightward shift in k is seen for spectra up to the end of prophase. The inset shows the variation of l^* with time, for three separate cells. The advent of correlations on smaller length scales as the cell moves into and through mitosis is evident. The sharp upturn in l^* at the end of mitosis (≈ 85 min from the start of the run) corresponds to the onset of metaphase.

nuclei have strong correlations in the organization of chromatin with a wavelength of about $4 \mu\text{m}$.

Cytoplasm does not contribute significantly to $S(k)$. As a check that the peaks in $S(k)$ were due to nuclear structures, we analyzed images of interphase cytoplasm near to and far from the nucleus (Fig. 3). There is a peak in $S(k)$ in regions $\approx 5 \mu\text{m}$ from the nucleus, but of an amplitude five times less than that obtained in nuclei and at a shorter wavelength of $k^* \approx 1.1 \mu\text{m}^{-1}$ (Fig. 3 hollow circles). These weak and shorter range correlations are most likely due to the rough ER, which is plainly visible in our images (data not shown), and are unrelated to the correlations generating the peaks in Fig. 2. In clear cytoplasm far from the nucleus, there are no correlations to be seen on the scale shown in Fig. 3 (hollow squares).

We also note that use of either 3D Fourier analysis or integration of 2D data over a number of z planes does not reveal any further information. In fact, we found that 3D analysis tends to mask the correlations clear in the 2D analysis. Because the chromosomes are essentially arranged in the x - y plane and occupy a roughly

$2\text{-}\mu\text{m}$ -thick region of the cell, any 3D analysis must be done by restricting the thickness of the cropping volume to only a few planes. Our 2D correlation peaks end up being simply broadened by out-of-focus light as the thickness of our cropping volume is increased. We conclude that the cells have essentially a 2D chromosome organization at the $\geq 0.3\text{-}\mu\text{m}$ scales relevant to light microscopy.

Compaction of interphase chromatin with trivalent cations. In order to observe the result of rapid “chemical” condensation of interphase chromatin, we microinjected trivalent cations (cobalt hexamine trichloride) in 60% PBS into interphase cells. This was done by penetrating the cell membrane with the micropipette and then pushing it up against the nuclear envelope. Injection was then done with the pipette essentially in contact with, but not punching through, the nuclear envelope.

Figures 4a–4i show a nucleus before, during, and after microinjection, in DIC. Initially, (Figs. 4a and 4b) the interphase chromatin has a patchy structure and is not visibly affected by the micropipette punching through the nuclear membrane. A small precursor burst of cobalt hexamine is used to test whether the pipette has indeed penetrated into the nucleus. In the first few seconds after microinjection long, sinuous, and clear “valleys” appear in the nucleus, cutting through the nuclear material. Simultaneously, in the region between two valleys, large mountainous inhomogeneities begin to develop (Figs. 4c and 4d). At longer times, the chromosomal material further lumps together into filaments of $\approx 1 \mu\text{m}$ in thickness, widening the valleys into lakes, and an overall radial pattern for the filaments and bounding clear regions begins to

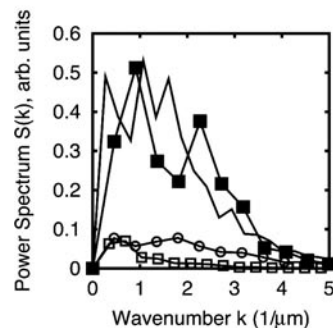


FIG. 3. Characterization of ambient, nonchromosomal, and non-nuclear correlations; circles show near-nuclear cytoplasmic inhomogeneities; open squares show distal cytoplasmic inhomogeneities; solid line shows correlations from interphase nucleus, while filled squares show mitotic chromosome correlations. Notice the shift in spatial correlation length for the near-nuclear cytoplasm (circles), due to correlations among densely packed nucleoli. The amplitude of distal scattering is negligible as the cytoplasm in this region is nearly clear.

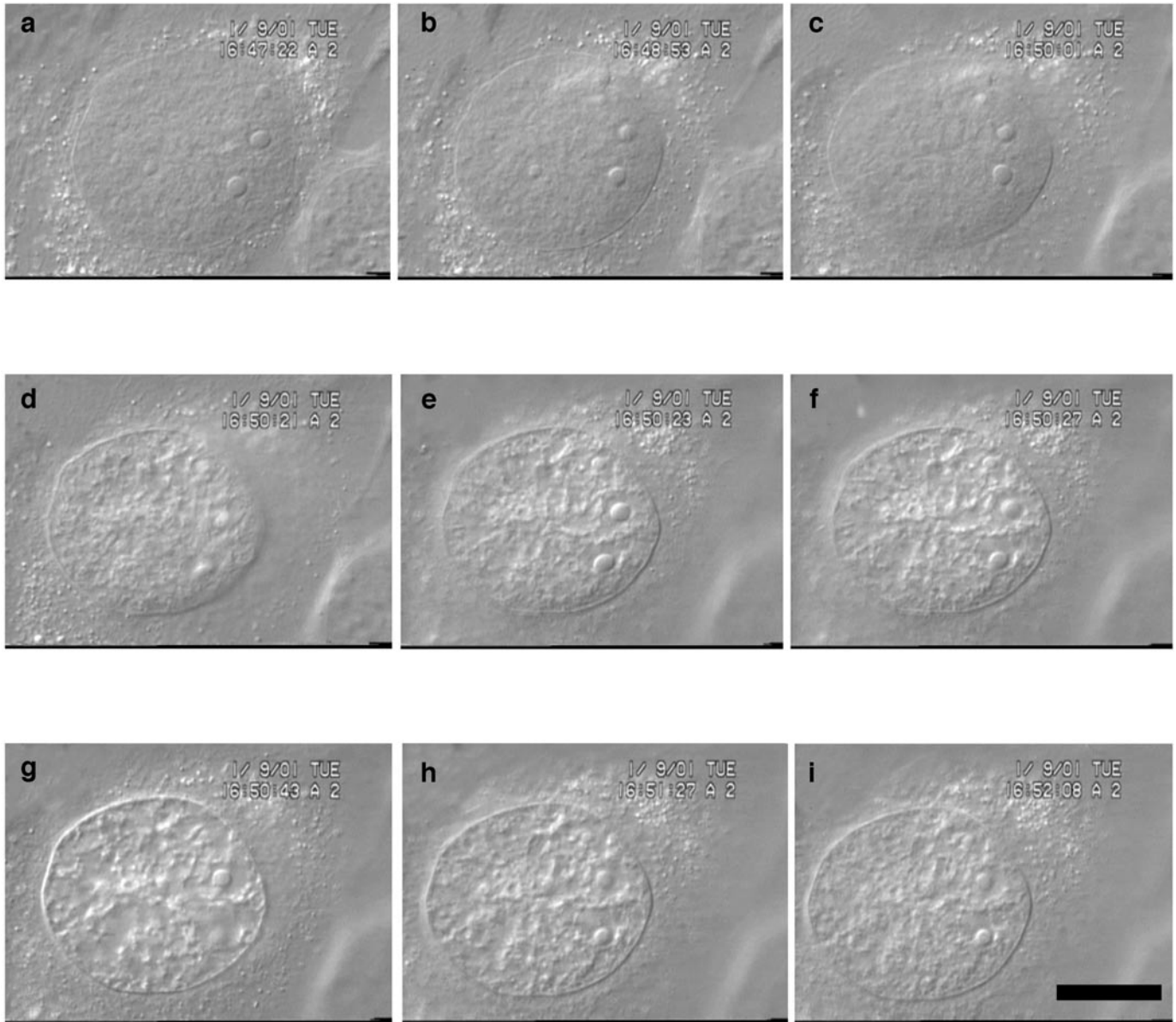


FIG. 4. Artificial compaction of interphase chromosomes using trivalent cations (cobalt hexamine trichloride). Photos show DIC images of the nucleus (a) 99 and (b) 8 s before microinjection. In (b), the pipette is lodged into the nucleus and a small amount of the cation has just been injected to ensure that the pipette is inside the nucleus. No major morphological changes arise yet. In (c), the nucleus has just been injected. We take this as our time origin. In (d) and (e), the nucleus is imaged 20 and 22 s after the microinjection, respectively. The landscape begins to roughen and become more lumpy. Voids or clear regions, apparently devoid of chromosomal material, are visible. Photos (f) and (g) show progressing condensation at 26 and 42 s after microinjection. By slide (g), the degree of artificial condensation has reached its maximum. The clear voids, barely visible in (e) and (f), are now a dominant morphological feature and outwardly radiating chromatin filaments about $1 \mu\text{m}$ thick are seen. The flow of ions is then stopped. Another 44 s later (h), the process has already reversed itself substantially, with the nucleus appearing as in (e). It takes another 61 s (i) for the nucleus to appear as in the early stages of condensation. The process completely reverses itself as all the cations diffuse out of the nucleus through the nuclear pores. See also: <http://safarsquid.phy.uic.edu/~mpoirier/experiments> and click on "Condensation of interphase chromosomes inside the nucleus by cobalt hex-amine tri-chloride" to view the movie from which the data are extracted. Bar is $20 \mu\text{m}$.

emerge. As the cations diffuse out of the nucleus, the chromatin begins to decondense as if the montage of images were being seen in reverse order (Figs. 4h and 4i). Inside the voids, small particles undergoing free diffusion are observed in the interchromosomal void

regions, indicating that they are essentially free of dense structure.

The qualitative results on chemical condensation of chromosomes, described above and shown in Fig. 4 (also see <http://safarsquid.phy.uic.edu/~mpoirier/>

experiments for a movie of the data), indicate that interphase chromatin domains are remarkably free to reorganize on 1-s time scales and that when chemically condensed, interphase chromatin reorganizes into thick filaments inside the nucleus. We originally hoped to carry out quantitative image analysis of the results, but unfortunately phase-contrast images of experiments similar to those of Fig. 4 produce images with strong “halos,” an artifact characteristic of phase-contrast imaging of samples with overly large density gradients. Analysis of phase-contrast data from experiments like Fig. 4 does, however, reveal the appearance of a power spectrum peak during artificial condensation. This peak has a spatial wavelength equal to the approximately 4- μm spacing of the condensed fibers of Fig. 4.

The DIC images, on the other hand, are difficult to analyze in the way we have done for natural cell division images (Figs. 1–3) because of the complicated correspondence between image brightness and nucleic acid + protein density. We hope to develop software suited to the analysis of DIC data and also to use fluorescent labeling techniques to get a clearer idea of how the interphase nucleus is reorganized by chemical condensation agents.

DISCUSSION

We have presented three types of experiments which, when taken together, indicate that chromosomes have a fiberlike structure which evolves from an expanded interphase form to a condensed prophase form. First, we have shown that during interphase, there is a characteristic correlation length associated with variations in chromatin density. Second, we have shown that during chromosome condensation, this correlation length at first stays fixed while the correlation strength intensifies. During late prophase the correlation length gradually decreases.

Finally, we used a chemical microinjection experiment to collapse chromatin during interphase and found that chromosomes are able to rapidly compact into fibers of dimensions similar to those of prophase chromosomes. This suggests that interphase chromatin domains are free to reorganize over few-micrometer distances, but are overall organized along filamentous tracks in the nucleus spaced by a few micrometers. This last experiment contradicts what would be expected if chromosomes were held in place by a dense nucleoskeleton with submicrometer pore sizes (“nuclear matrix”), unless that nucleoskeleton was capable of being disassembled on <1-s times in response to trivalent cations.

A far simpler explanation for the trivalent cation injection results is that interphase chromosomes and prophase chromosomes are closely related in structure, having in common a fiberlike structure. This model

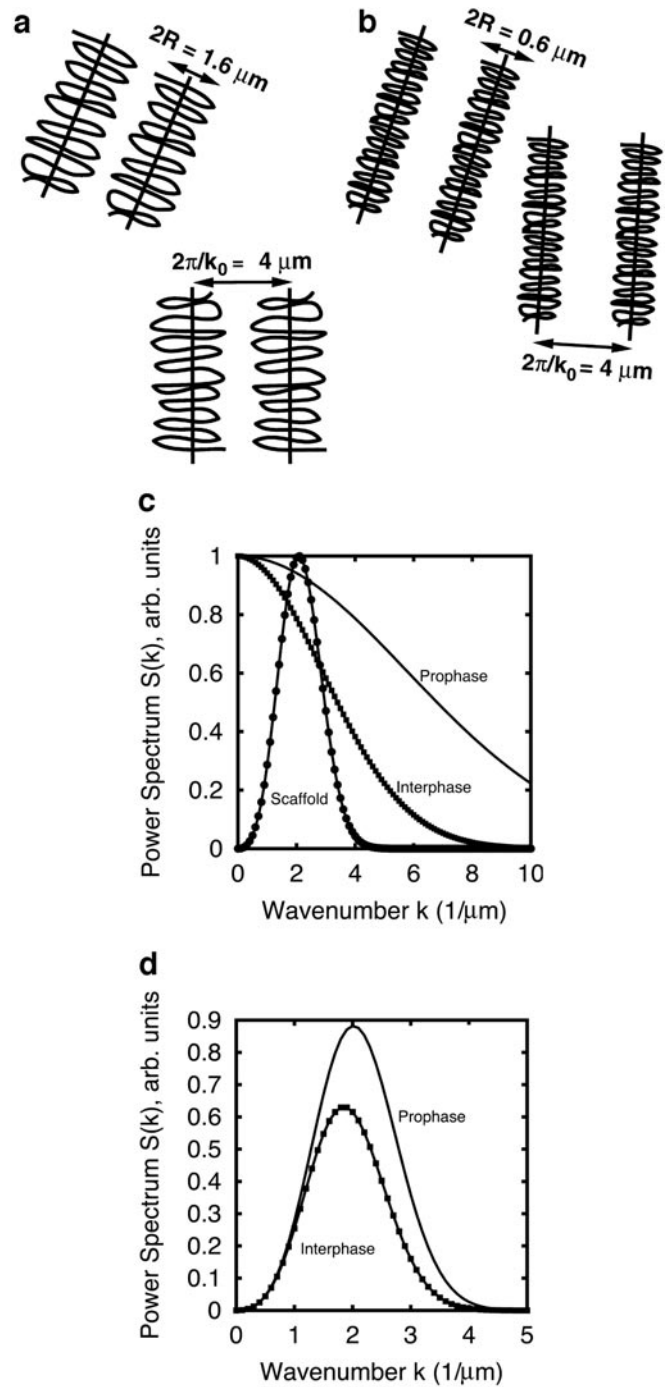


FIG. 5. Illustration of our model for the dynamics of I^* as a cell moves through interphase to prophase. Figures a and b are cartoons of chromosome organization in interphase and mitosis (late prophase), respectively. Chromosomes are more compacted in b, which results in broadening of $\phi(k)$, as shown in c (solid line) relative to the interphase loop distribution (c, squares). The peak position of $\rho(k)$, the convolution of the loop and scaffold power spectra, shifts to the right as a consequence from d (filled squares) for interphase to d (solid) for prophase. R goes from $0.8 \mu\text{m}$ in interphase to $0.3 \mu\text{m}$ in prophase for a loop of 100 statistical segments. For the fiber axis distribution, $k_0 = 1.4 \mu\text{m}^{-1}$ and δ is 0.6 times k_0 .

adopts the point of view that the main structural difference between interphase chromosomes and late prophase chromosomes is the degree to which chromatin segments are compacted. Below we develop this model quantitatively to show how it can explain our results (Fig. 5).

Loop-compactation model. We suppose that inside the nucleus the chromosome fiber axis has a spatial density distribution $\psi(r)$. We expect these axes to be locally linear structures, whose average spacing roughly defines the characteristic length observed. We therefore assume the fiber axes to have a peaked power spectrum,

$$|\psi(k)|^2 = Ak^2 \exp\left[\frac{-(k - k_0)^2}{2\delta^2}\right], \quad (4)$$

with A an overall amplitude. Here k_0 is the wave number corresponding to the spacing between adjacently packed fibers. The peaked form of ψ does not imply any global ordering of the chromosome axes, but only the local organization imposed by the constraint that they do not run into each other. The parameter δ is the width (in μm^{-1}) of our fiber axis distribution in Fourier space.

From each point of the fiber axis hang chromatin loops, whose spatial mass distribution we take to be the free end distribution of a Gaussian polymer tethered at r' [14],

$$\phi(r - r') = \left(\frac{3}{2\pi R^2}\right)^{3/2} \exp\left[\frac{-3(r - r')^2}{2R^2}\right]. \quad (5)$$

The parameter R is the typical size of the loops: we can make loops disperse ($R \rightarrow \infty$) or arbitrarily compacted ($R \rightarrow 0$). For other animal cells, chromatin loops are observed in the 100-kb range [15], suggesting a rough range for R from 600 nm (disperse) to 300 nm (compact) [these limits on R correspond to a dispersed random-walk estimate ($R \approx bN^{1/2}$) vs a compact blob of chromatin segments ($R \approx bN^{1/3}$), where $b \approx 60$ nm is the statistical segment length of chromatin fiber as determined in [16]].

Using this simple model we can compute the chromatin power spectrum by forming the convolution of ϕ with ψ . In terms of the Fourier-transformed chromosome axis and loop mass distributions the chromatin power spectrum is $S(k) = |\rho(k)|^2 = |\psi(k)|^2 |\phi(k)|^2$:

$$S(k) = Ak^2 \exp\left[\frac{-(k - k_0)^2}{2\delta^2}\right] \exp\left[\frac{-R^2 k^2}{3}\right]. \quad (6)$$

The position of the peak of the product of the exponentials in Eq. (6), $k^* = k_0/(1 + 2R^2\delta^2/3)$, is modulated by the compaction parameter R .

In the disperse limit $R \rightarrow \infty$, the fiber axis correlations are washed out by overlapping chromatin domains, whose spectra in reciprocal space are more localized near $k = 0$. The result is a shift in the peak of $S(k)$ toward $k = 0$ from k_0 . In the opposite compacted limit $R \rightarrow 0$, the chromatin domains are strongly compacted onto the chromosome axis, causing their Fourier space distribution to be broadened. This leads to the convolution having its peak near k_0 as $R \rightarrow 0$. As R is varied over a range between these limits, $k^*(R)$ shifts over a range between 0 and k_0 . A marked variation in peak height is also observed in our model. While a similar although smaller effect is seen in the experimental data, the exact amplitude in the observed spectra may be modulated by other factors. Figure 5 shows results for this model, and it can be seen that with reasonable choices for R and the functional form of the chromosome fiber axis and chromatin loop structure factors, we can roughly reproduce the variation in $k^*(R)$ observed experimentally during prophase.

This model is consistent with other experimental facts about interphase and mitotic chromosome structure. Random-walk chromatin fiber behavior as observed in interphase [3] is generated by our $\phi(r)$. The underlying fiberlike structure in ψ is consistent with the territories observed by Cremer *et al.* [1]. Finally, the loop compaction picture is essentially the reverse of what was observed in classical chromatin dispersal/“scaffold” visualization experiments [8].

Finally we note that the compaction assumed in this model need not come from self-adhesion of chromatin itself (as we have artificially induced using trivalent cations). Separate experiments clearly indicate that mitotic chromatin does not behave as if it is a self-cohesive solid (e.g., mitotic chromosomes have a Poisson ratio ≈ 0.1 , far below the 0.5 expected for a solid elastic body) [17, 18]. In lieu of self-adhesion, the compaction of mitotic chromatin during prophase might be generated by chromatin–chromatin connectors which crosslink chromatin into a compact configuration during mitosis, as suggested in [7]. We emphasize that our model and experimental results do not require a contiguous protein scaffold, but only a well-defined fiberlike chromosome architecture.

This research was supported by NSF Grant DMR-9734178, by a grant from the Petroleum Research Foundation, by a Research Innovation Award from the Research Corporation, by a Biomedical Engineering Research Grant from the Whitaker Foundation, by a Focused Giving Grant from Johnson & Johnson Corporate Research, and by the University of Illinois Foundation.

REFERENCES

1. Cremer, T., Kurz, A., Zirbel, R., Dietzel, S., Rinke, B., Schnock, E., Speicher, M. R., Mathieu, U., Jauch, A., Emmerich, P., Scherthan, H., Ried, T., Cremer, C., and Lichter, P. (1993). Role of chromosome territories in the functional compartmentaliza-

- tion of the cell nucleus. *Cold Spring Harbor Symp. Quant. Biol.* **LVIII**, 777–792.
2. Yokota, H., van den Engh, G., Hearst, J. E., Sachs, R., and Trask, B. J. (1995). Evidence for the organization of chromatin in megabase pair-sized loops arranged along a random walk path in the human G0/G1 interphase nucleus. *J. Cell Biol.* **130**, 1239–1249.
 3. Marshall, W. F., Dernburg, A. F., Harmon, B., Agard, D. A., and Sedat, J. W. (1996). Specific interactions of chromatin with the nuclear envelope: Positional determination within the nucleus in *Drosophila melanogaster*. *Mol. Biol. Cell* **7**, 825–842.
 4. Wolffe, A. P. (1995). "Chromatin," 2nd ed. Sect. 2.4, Academic Press, New York.
 5. Koshland, D., and Strunnikov, A. V. (1995). Mitotic chromosome condensation. *Annu. Rev. Cell. Dev. Biol.* **12**, 305–333.
 6. Strunnikov, A. V. (1998). SMC proteins and chromosome structure. *Trends Cell Biol.* **8**, 454–459.
 7. Hirano, T. (2000). Chromosome cohesion, condensation, and separation. *Annu. Rev. Biochem.* **69**, 115–144.
 8. Earnshaw, W. C., and Laemmli, U. K. (1983). Architecture of metaphase chromosomes and chromosome scaffolds. *J. Cell Biol.* **96**(1), 84–93.
 9. Belmont, A. S., Sedat, J. W., and Agard, D. A. (1987). A three-dimensional approach to mitotic chromosome structure: Evidence for a complex hierarchical organization. *J. Cell Biol.* **105**(1), 77–92.
 10. Bates, F. S., and Wiltzius, P. (1989). Spinodal decomposition of a symmetric critical mixture of deuterated and protonated polymer. *J. Chem. Phys.* **91**(5), 3258–3274.
 11. Widom, J., and Baldwin, R. L. (1983). Monomolecular condensation of lambda-DNA induced by cobalt hexamine. *Biopolymers* **22**(6), 1595–1620.
 12. Rieder, C. L., and Hard, R. (1990). Newt lung epithelial cells: Cultivation, use, and advantages for biomedical research. *Int. Rev. Cytol.* **122**, 153–220.
 13. Reese, D. H., Yamada, T., and Moret, R. (1976). An established cell line from the newt *Notophthalmus viridescens*. *Differentiation* **6**, 75–81.
 14. Doi, M., and Edwards, S. F. "The Theory of Polymer Dynamics," Sect. 2.1, Oxford Univ. Press, Oxford.
 15. Jackson, D. A., Dickinson, P., and Cook, P. R. (1990). The size of chromatin loops in HeLa cells. *EMBO J.* **9**, 567–71.
 16. Cui, Y., and Bustamante, C. (2000). Pulling a single chromatin fiber reveals the forces that maintain its higher-order structure. *Proc. Natl. Acad. Sci. USA* **97**, 127–132.
 17. Poirier, M., Eroglu, S., Chatenay, D., and Marko, J. F. (2000). Reversible and irreversible unfolding of mitotic newt chromosomes by applied force. *Mol. Biol. Cell* **11**, 269–276.
 18. Houchmandzadeh, B., Marko, J. F., Chatenay, D., and Libchaber, A. (1997). Elasticity and structure of eukaryote chromosomes studied by micromanipulation and micropipette aspiration. *J. Cell Biol.* **139**, 1–12.

Received August 28, 2001

Revised version received February 20, 2002